ChemPubSoc Europe

DOI: 10.1002/chem.201504975

CHEMISTRY
A European Journal
Full Paper

Supramolecular Electron Transfer

Supramolecular Photoinduced Electron Transfer between a Redox-Active Hexanuclear Metal–Organic Cylinder and an Encapsulated Ruthenium(II) Complex

Lu Yang, Cheng He,* Xin Liu, Jing Zhang, Hui Sun, and Huimin Guo*[a]

Abstract: By using redox-active nickel(II) ions as the connect nodes, a hexanuclear metal–organic cylinder (Ni-YL) was achieved through self-assembly with a large cavity and an opening windows capable to accommodate guest molecules. The suitable cavity of Ni-YL provides an opportunity to encapsulate the anionic ruthenium bipyridine derivative $[Ru(dcbpy)_3]$ (dcbpy = 2,2′-bipyridine-4,4′-dicarboxylic acid) as the photosensitizer for light-driven reactions. The host–guest behavior between Ni-YL and $[Ru(dcbpy)_3]$ was investigated by mass spectrometry, NMR spectroscopy, and computational studies, revealing an effective binding of the guest $[Ru(dcbpy)_3]$ within the cavity of Ni-YL. Optical experiments suggested a pseudo-intramolecular photoinduced electron transfer (PET) process between the $[Ru(dcbpy)_3]$ and the host Ni-YL, leading to an efficient light-driven hydrogen production based on this system. Control experiments with a mononuclear Ni complex as a reference photocatalyst and the inactive $[Fe(dcbpy)_3]$ as an inhibitor for comparison were also performed to confirm such a supramolecular photocatalysis process.

Introduction

Binding a specific guest molecules within the cavity of host molecules is one of the classical issues, which have drawn continuous attentions in the supramolecular chemistry.[1] The hosts can be well modified with functional interaction sites and well-defined inner void spaces by ingenious design and construction, usually defined as molecular containers for their ability to accommodate other chemical species.[2,3] The excellent and well-studied hosts in this field were mainly focus on macrocycles formed through covalent bonds, including cyclodextrins, calixarenes, covalent capsules, and cucurbiturils, which have been widely delineated by the pioneering work of many groups.[4] During the last decades, another kind of interesting molecular hosts, the coordination-driven self-assembled metal–organic polyhedra (MOPs) containing internal cavities with well-defined shapes and sizes, have achieved increasing prominence.[5] Owing to their promising functionalities as artificial metalated host platforms, it is possible for these molecular hosts to mimic protein receptors or enzymes for their abilities to effectively bind substrates, stabilize reactive intermediates, and catalyze chemical transformations.[6]

On the other hand, a rising interest in reactions driven by photoinduced electron transfer (PET), in particular, for the production of solar fuels, presents opportunities to design new systems that absorb visible light and exhibit favorable redox chemistry for photosensitization. The construction of host–guest supramolecular photosynthetic systems would enforce the electron transfer process in a local microenvironment,[7] thus the pseudo-intramolecular electron and energy transfer could be modified to avoid unwanted electron transfer processes. In this case, the introduction of metal ions would endow metallosupramolecular hosts with excellent redox-active properties for the PET process, together with their benign host–guest behavior, that the MOP system could act as a kind of potential model in photo-redox reactions.[8]

Herein, we report a new cationic hexanuclear metal–organic cylinder (Ni-YL) as a host for the encapsulation of anionic trisbipyridine ruthenium derivatives, by incorporating the Ni^{II} ions as construction nodes and the flexible YL ligand, containing amide and secondary amino groups as trigger sites (Figure 1 a). The tris(bipyridine)ruthenium(II) complex and its derivatives are known for their excellent photophysical and excited-state redox properties.[9] The encapsulation of such complexes within a well-designed supramolecular system could bring fruitful applications in the photochemical field. We envisioned that the extremely flexible backbone and the large cavity of the host, coupled with the potential hydrogen-bonding interactions would provide an opportunity to construct suitable architectures to encapsulate this widely used photosensitizer. And the introduction of the well-coordinated nickel ion as the connect nodes was expected to exhibit suitable redox-active properties for proton reduction and the complexation species

[a] L. Yang, Prof. C. He, Dr. X. Liu, J. Zhang, H. Sun, Dr. H. Guo
State Key Laboratory of Fine Chemicals
Dalian University of Technology
Dalian, 116023 (P. R. China)
Fax: (+86) 411-84986261
E-mail: hecheng@dlut.edu.cn
guohm@dlut.edu.cn

Supporting information for this article is available on the WWW under http://dx.doi.org/10.1002/chem.201504975.

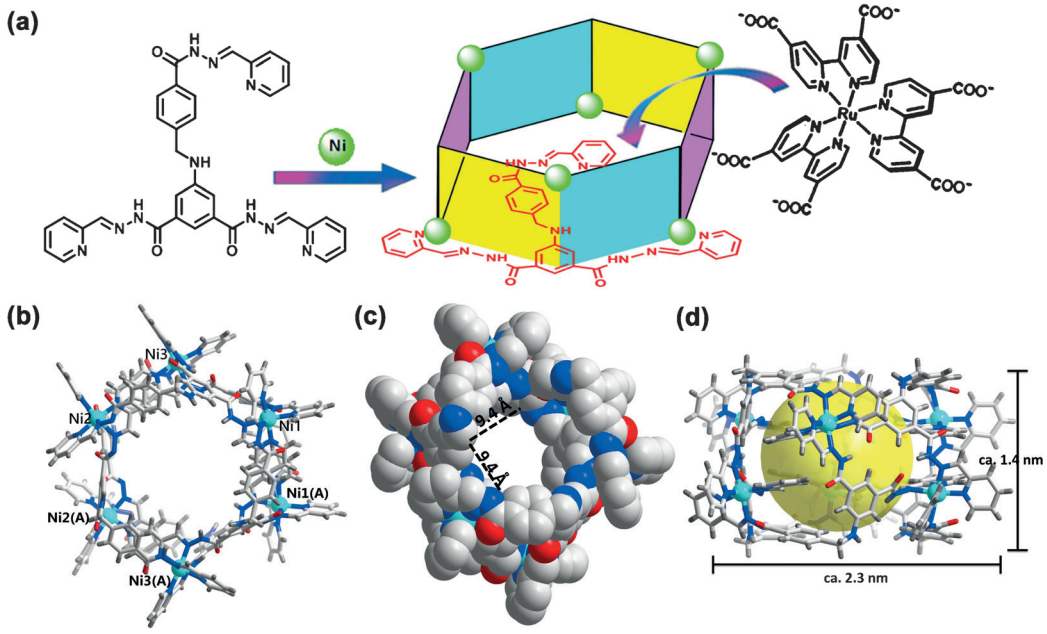

Figure 1. a) Representation of the assembly of the metal–organic cylinder host Ni-YL and the encapsulation of the anionic [Ru(dcbpy)$_3$] (dcbpy = 2,2′-bipyridine-4,4′-dicarboxylic acid) through host–guest behavior. b) Molecular structure of Ni-YL from the top view; c) Space-filling representation of the vast cavity of the cylinder Ni-YL. d) Side view of Ni-YL. Solvent molecules and anions are omitted for clarity. Symmetry code A: $-x-1,-y-1, z$.

greatly improved the efficiency of the proton transfer within the well-defined microenvironment.

Results and Discussion

The backbone of the ligand YL contains three amide groups and one secondary amine group that linked by 4-carbohydrazide and 5-amino-isocarbohydrazidebenzene. The ligand was prepared by reaction of 5-(4-(hydrazinecarbonyl)benzylamino)isophthalohydrazide with 2-pyridinecarboxaldehyde under heating to reflux in methanol. Vapor diffusion of diethyl ether into the mixture of the ligand and $Ni(BF_4)_2{\cdot}6H_2O$ in acetonitrile led to the crystallization of the cylinder Ni-YL (Scheme 1). The ESI-MS spectrum of Ni-YL in acetonitrile solution exhibits four main bunches of peaks at $m/z = 923.80$, 941.40, 1176.25, and 1198.25, assigned to the species $[Ni_6YL_6{\cdot}6(BF_4)\text{-}H]^{5+}$, $[Ni_6YL_6{\cdot}7(BF_4)]^{5+}$, $[Ni_6YL_6{\cdot}7(BF_4)\text{-}H]^{4+}$, and $[Ni_6YL_6{\cdot}8(BF_4)]^{4+}$, respectively. This result suggested that the formation and stable existence of a $[Ni_6YL_6]$ complex in solution. Single-crystal X-ray diffraction revealed that the assembly of six Ni^{II} ions and six ligands formed the large cationic hexanuclear cylinder Ni-YL approximately with a length of 2.3 nm and a height of 1.4 nm (Figure 1). All the three-armed ligands connect to three different nickel ions, where the six nickel ions each coordinate with three different ligands as the NN bidentate chelators in an octahedral geometry. Thus, the amide groups are coordinated free due to the rotation of the C=O group, unlike with the previous reported ligands of amide groups involved tridentate

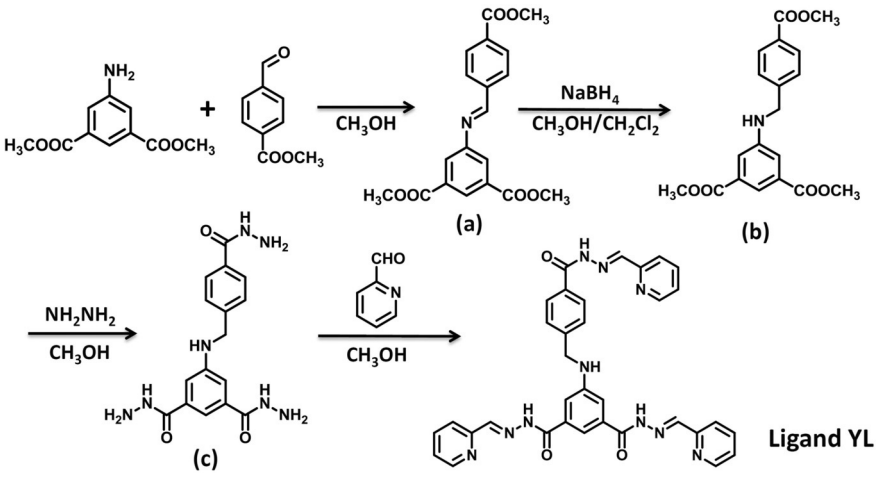

Scheme 1. Synthetic route to the ligand YL.

chelators by our group.[10] The flexible ligand can be represented as a tripod with the central secondary amine group as the vertex. One arm of a ligand is bound to one Ni ion in one layer, whereas the other two arms are connected to two ions in the other layer. From the side view of the cylinder, the six nickel ions are positioned at two different layers that are formed by three of the coplanar nickel ions, and the three nickel ions in the same layer present a triangle configuration with the edge distance ranging from approximately 14.7–15.1 Å. The distances of the C=O and C–N bonds in the ligand backbone are intermediate between formal single and double bonds, suggesting the extensive delocalization over the whole skeleton.[11] According to the single-crystal X-ray diffraction analysis, there are only eight BF_4^- counterions to balance the positive charge in Ni-YL, and thus four protons of the skeleton are delocalized during the crystallization.

Notably, the structure of Ni-YL is similar to the classic covalent host cucurbit[6]uril molecule and its derivatives, both of which are hexameric species and possess cylindrical cavities. The cucurbit[6]uril molecule contains twelve high active C=O groups sequentially arranged along the margins of the cylinder exhibiting the binding ability toward the substrate,[12] whereas in Ni-YL, there are eighteen free amide groups and six secondary amines, which could act as hydrogen-bonding interaction sites. Moreover, the opening window of the Ni-YL cavity is about 9.4 Å (Figure 1 c), which is much larger than that of the cucurbit[6]uril molecule (5.8 Å) and even comparable to the diameter of the cucurbit[8]uril molecule, which is 8.9 Å. But the external diameters of Ni-YL and cucurbit[6]uril are close to each other, showing that Ni-YL possesses a broader opening window to accommodate the guests to access. The positively charged cylinder could provide a restrained inner space to the capsules, together with the rotatable secondary amine groups and intact amide groups that act as possible hydrogen-bond interaction sites. Thus, we expected that Ni-YL could be a promising metal–organic macrocycle host, like the cucurbit[6]uril molecule and its derivatives,[13] possessing a high host–guest behavior with high affinity and selectivity toward the specific substrates.[14]

The carboxylic derivative of tris(bipyridine)ruthenium(II), $[Ru^{II}(dcbpy)_3]^{2+}$ (the forms with proton or anionic species united as $[Ru(dcbpy)_3]$ below) represents an ideal guest in our system not only because of its appropriate size and excellent photophysical properties, but also based on the fact that it exists in an anion form in alkaline medium that could interact with the positive-charged host driven by electrostatic attraction. The host–guest behavior of binding $[Ru(dcbpy)_3]$ was firstly investigated by ESI spectrometry. The addition of an equimolar amount $[Ru(dcbpy)_3]$ into an acetonitrile solution of Ni-YL in the presence of TEOA (triethanolamine) exhibited several new peaks at $m/z = 1072.60$, 1090.20, 1340.50, and 1384.50 (marked with asterisks in Figure 2). Comparing the simulation results based on natural isotopic abundances, these peaks were assigned to $[Ni_6YL_6{\cdot}Ru(dcbpy)_3{\cdot}5(BF_4)\text{-}4H]^{5+}$, $[Ni_6YL_6{\cdot}Ru(dcbpy)_3{\cdot}6(BF_4)\text{-}3H]^{5+}$, $[Ni_6YL_6{\cdot}Ru(dcbpy)_3{\cdot}5(BF_4)\text{-}5H]^{4+}$, and $[Ni_6YL_6{\cdot}Ru(dcbpy)_3{\cdot}7(BF_4)\text{-}3H]^{4+}$, respectively (Figure 2), confirming the formation of a 1:1 stoichiometric

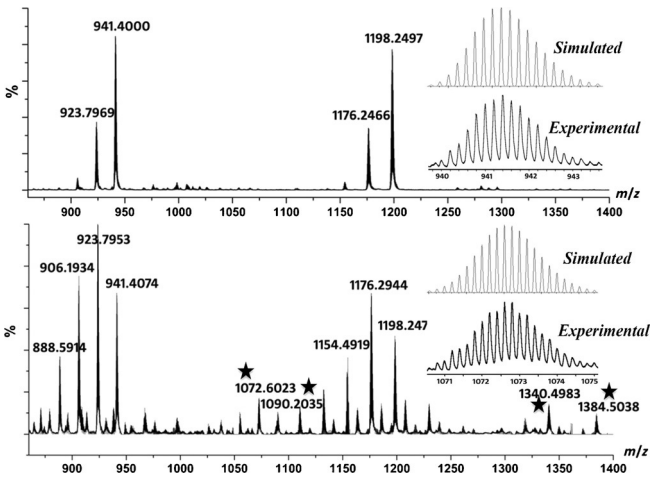

Figure 2. ESI-MS spectra of Ni-YL in acetonitrile solution (top) and of $[Ru(dcbpy)_3]$ in methanol solution mixed with the aforementioned solution (bottom). The insets show the measured and simulated isotopic patterns at $m/z = 941.4000$ (top) and 1072.6023 (bottom), respectively.

complexation species $[Ni\text{-}YL{\cdot}Ru(dcbpy)_3]$. Moreover, the ^1H NMR titration of $[Ru(dcbpy)_3]$ (Figure S8 in the Supporting Information) also in CD_3CN and D_2O (1:1) upon addition of one mole ratio Ni-YL in the above-described solution exhibited a significant downfield shifts of the protons ($\Delta\delta = 0.19$, 0.45 and 0.04 ppm, respectively). These shifts provide another indicator for the encapsulation of the anionic $[Ru(dcbpy)_3]$ within the suitable pocket of the cylinder Ni-YL forming the host–guest complexation species $[Ru(dcbpy)_3]\subset$Ni-YL.

Extensive molecular force field-based calculations were performed to get a possible picture of the cationic Ni-YL cylinder and the $[Ru(dcbpy)_3]\subset$Ni-YL encapsulation starting from the crystal structures of Ni-YL and $[Ru(dcbpy)_3]$ in water solution by using universal force field as implemented in the program Gaussian 09.[15] Frequency analysis was also carried out to ensure that the calculated structures are real minima on the potential energy surface (Figure 3). In the most plausible structure of Ni-YL, the averaged Ni–Ni distance is 14.90 Å falling in the experimental range of approximately 14.7–15.1 Å and the diameter of the cavity on top of the cylinder is 9.78 Å with a diagonal of 17.62 Å. The large size of the cavity ensures the encapsulation of the $[Ru(dcbpy)_3]$, in which the largest O–O distance is 13.84 Å. There is no significant structure change observed on Ni-YL in the plausible structure of the encapsulation. In fact, the $[Ru(dcbpy)_3]$ fully utilizes the apertures on the side walls of Ni-YL to release the tension. At the same time, one of the dcbpy ligand is reoriented to be parallel to the neighboring YL ligand and the nearest distance is 3.75 Å, which is typical for π–π stacking interactions among aromatic molecules. At the same time, close contacts were also observed between the carboxyl groups of the dcbpy ligand and the N–H moiety of the Ni-YL and the nearest O–H distance is only 2.61 Å, which is typical for hydrogen bonds. These interactions may each play a role in promoting the encapsulation thermodynamically and remaining the stability of the complexation. These results could by related to the NOESY spectrum of the

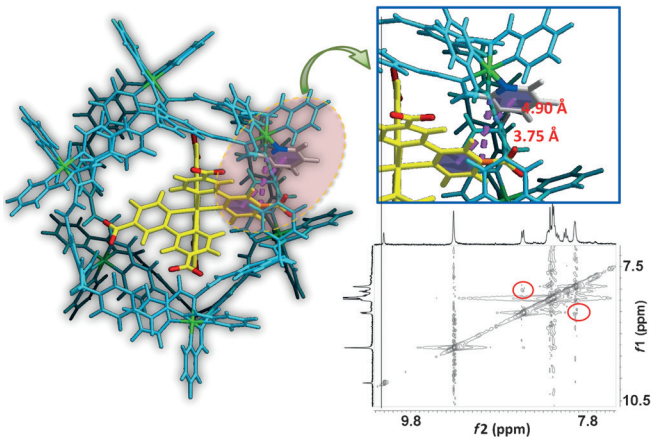

Figure 3. Representation of the encapsulation of Ni-YL and [Ru(dcbpy)$_3$] computed by molecular force field-based calculations and partial NOESY spectroscopy of the two components in the mixture of D_2O and [D_3]acetonitrile.

mixture of [Ru(dcbpy)$_3$] and Ni-YL with equal stoichiometric ratio, which indicates the H–H interactions between the two components, namely the protons of the pyridine rings of the [Ru(dcbpy)$_3$] and the skeleton of cylinder (red circles in Figure 3).

Cyclic voltammograms (CVs) of Ni-YL in acetonitrile solution displayed a Ni^{II}/Ni^{I} reduction wave at −0.75 V (vs. Ag/AgCl) with a scan rate of 100 mV s^{-1}.[16] The addition of TEOA·HCl with increasing amounts triggers the appearance of a new irreversible wave near the Ni^{II}/Ni^{I} response (Figure 4a). Increasing the TEOA·HCl concentration raises the height of the new wave and shifts it to more negative potentials whereas the Ni^{II}/Ni^{I} reversible wave disappeared. The new wave is assignable to the typical proton electroreduction, suggesting that Ni-YL is able to reduce protons through a catalysis process. In order to construct stable host–guest complexation species with the cationic host Ni-YL, the [Ru(dcbpy)$_3$], which has a suitable redox potential[17] under basic condition, was chosen as the photosensitizer.

Fluorescence titration revealed that the addition of Ni-YL in a solution of [Ru(dcbpy)$_3$] caused significant emission quenching (Figure 4b). The quenching process is easily attributed to a classical photoinduced electron transfer from the excited state $*Ru^{II}$ to the redox catalyst Ni-YL.[18] Ni-YL thus is able to be activated directly for the proton reduction by the excited state $*Ru^{II}$. The luminescence of a solution of [Ru(dcbpy)$_3$] (10.0 μM) in H_2O/EtOH (1:1) at $\lambda = 620$ nm containing Ni-YL (20.0 μM) decays in an exponential fashion with a lifetime of 1.06 μs similar to that of a pure [Ru(dcbpy)$_3$] solution (1.07 μs, Figure S13 in the Supporting Information). It seems that two luminescent species coexist, namely, the [Ru(dcbpy)$_3$] moiety itself with its fluorescent lifetime being maintained, and the host–guest complexation species [Ru(dcbpy)$_3$]⊂Ni-YL in the titration mixture. The fact that the decay behavior approximates well to a typical exponential function suggests that the complexation species exhibits an ignored emission. The titration profile of [Ru(dcbpy)$_3$] (10.0 μM) upon addition of Ni-YL up to 50.0 μM is consistent with a Hill plot.[7c] The best fitting of the titration profile suggests a 1:1 host–guest behavior with an association constant (K_{ass}) of $(6.46 \pm 0.13) \times 10^4$ M^{-1}.

In a typical light-driven reduction system containing the photocatalyst Ni-YL, the photosensitizer [Ru(dcbpy)$_3$], and the electron donor TEOA, there are two possible reaction pathways. One of the pathways is the excited state of [$*Ru^{II}$(dcbpy)$_3$] being reduced by the TEOA to [Ru^{I}(dcbpy)$_3$] through a reductive quenching process, then the electron is transferred from the [Ru^{I}(dcbpy)$_3$] species to the Ni-YL catalyst and a possible proton reduction could occur on the catalyst. Another way is that the electron is directly transferred from the [$*Ru^{II}$(dcbpy)$_3$] to the catalyst Ni-YL, and the following step should be that the [Ru^{III}(dcbpy)$_3$] species are reduced by TEOA. Both the two processes are thermodynamically feasible in our system, the PET process of [Ru(dcbpy)$_3$] (40.0 μM) with Ni-YL (40.0 μM) in the presence of TEOA (15% in volume) was then investigated by transients absorption studies (Figure 5a, blue line). The spectrum recorded 2.4 μs after the laser flash showed a peak at $\lambda = 420$ nm corresponding to the maximum absorption of Ru^{III} ions,[19] and no absorption of Ru^{I} ions was observed 6 μs after the laser flash, indicating the direct PET process from the excited state $*Ru^{II}$ to the Ni^{II} centers to form Ru^{III} species was happened under this light-driven condition.

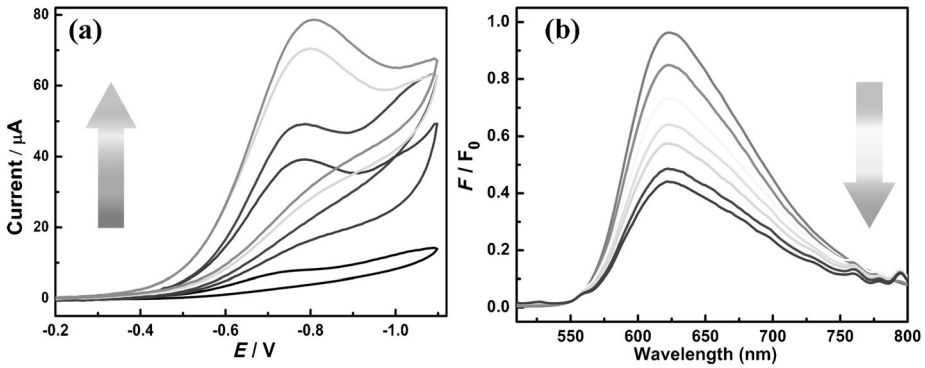

Figure 4. a) Cyclic voltammograms of Ni-YL (1 mM) upon addition of 2.0, 4.0, 6.0, and 8.0 equivalents of TEOA·HCl in CH_3CN solution containing $TBAPF_6$ (TBA = tetrabutylammonium) (0.1 M). b) The emission quenching of [Ru(dcbpy)$_3$] (10.0 μM) upon the addition of Ni-YL in EtOH/H_2O (1:1) at pH 10.5.

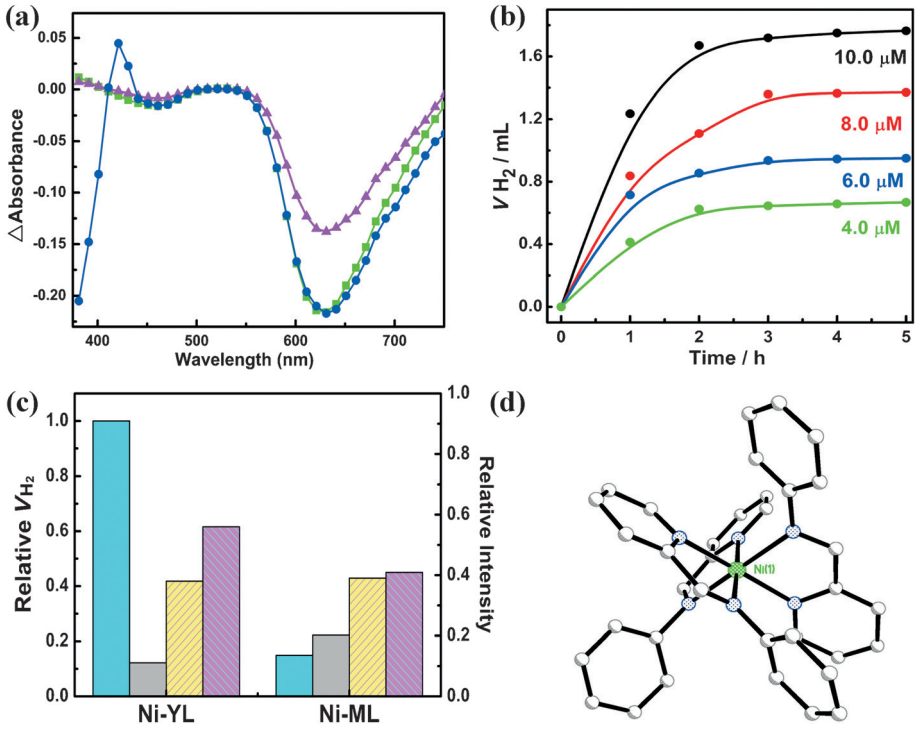

Figure 5. a) Transient absorption spectra of [*Ru(dcbpy)$_3$] in the presence of TEOA (15%, pink line) and Ni-YL (40.0 μM, blue line) or Ni-ML (0.24 mM, green line) in H_2O/EtOH (1:1) solution at 298 K recorded 2.4 μs after the laser flash. b) H_2 production upon irradiation of the system containing TEOA (15%), pH 10.5 and [Ru(dcbpy)$_3$] (2.0 mM) with different concentrations of Ni-YL. c) Histogram of the H_2 production of the systems containing Ni-YL (10.0 μM) or Ni-ML (60.0 μM), respectively, TEOA (15.0%) and [Ru(dcbpy)$_3$] (2.0 mM) at pH 10.5 (cyan bar), after the addition of 2.0 mM [Fe(dcbpy)$_3$] (gray bars) as inhibitor, and the normalized emission intensity of 10.0 μM [Ru(dcbpy)$_3$] (yellow bar) upon addition of Ni-YL (50 μM) or Ni-ML (0.3 mM), respectively, and of the recovery in the presence of 0.1 mM [Fe(dcbpy)$_3$] for Ni-YL (50 μM) and 0.6 mM [Fe(dcbpy)$_3$] for Ni-ML (0.3 mM) (pink bars). The intensities were recorded at $\lambda = 620$ nm, excitation at $\lambda = 470$ nm. d) Crystal structure of Ni-ML.

To further investigate whether the existence of the supramolecular species [Ru(dcbpy)$_3$]⊂Ni-YL indeed influence the PET process for light-driven H_2 generation, the mononuclear complex Ni-ML exhibiting the similar coordination mode of the Ni centre as within Ni-YL was synthesized as a reference (Figure 5d). The CV of Ni-ML revealed a reduction peak assignable to the Ni^{II}/Ni^{I} process ($E_{1/2} = -0.78$ V) exhibiting a similar redox potential than that of Ni-YL. The process of the fluorescence of [Ru(dcbpy)$_3$] quenched by Ni-ML is consistent with a Stern–Volmer profile with a Stern–Volmer constant (K_{sv}) of $(1.95 \pm 0.13) \times 10^3\ M^{-1}$ (Figure S12 in the Supporting Information). The decrease of the emission lifetime (from 1.07 to 0.86 μs) of [Ru(dcbpy)$_3$] (10.0 μM) with addition of Ni-ML (0.12 mM) suggested that the photoinduced electron transfer displayed in a normal bimolecular manner. The transients absorption spectrum recorded 2.4 μs after the laser flash of [Ru(dcbpy)$_3$] with Ni-ML did not show the characteristic absorption of Ru^{III} ions, but after 6 μs the absorption of Ru^{I} ions was observed, demonstrating that an excited-state reduction quenching of [Ru(dcbpy)$_3$] by TEOA clearly dominates the light-driven process.

From a mechanistic point of view, the encapsulated molecules of [Ru(dcbpy)$_3$] inside the pocket of Ni-YL enforce the proximity between the nickel-based redox catalytic sites and the photosensitizer. This supramolecular system then allows a direct photoinduced electron transfer process from the excited-state $*Ru^{II}$ to the redox catalyst.[20] The close proximity between the redox sites and the photosensitizer within the confined space further encourages the PET process in a more powerful pseudo intramolecular pathway.[21]

Irradiation of a solution containing [Ru(dcbpy)$_3$] (2.0 mM), Ni-YL (10.0 μM), and TEOA (15%) in a H_2O/EtOH (1:1) solution at 298 K resulted in a direct hydrogen generation. A common Xe lamp (500 W) was utilized as the light source by using a $\lambda =$ 400 nm filter to eliminate the effect of ultraviolet light. The highest efficiency of the H_2 production was achieved when the initial pH value was 10.5, whereas the ultimate pH value reduced to 10.2 after the irradiation. By fixing the concentrations of [Ru(dcbpy)$_3$] (2.0 mM) and TEOA (15%), the volume of the hydrogen produced holds a linear relationship with the concentrations of the catalyst Ni-YL ranging from 4.0 to 10.0 μM (Figure 5b). The initial turnover frequency (TOF) is about 1100 moles hydrogen per mole of catalyst per hour, and the calculated turnover number (TON) is about 1600 moles hydrogen per mole of catalyst. This TON value was compared to some previously reported Ru/TM (transition-metal) systems.[22] Control experiments were carried out without the photocatalyst or without [Ru(dcbpy)$_3$] or without TEOA under the optimal conditions, which suggested that the absence of any component could hardly trigger the process of the proton reduction to H_2. When using the YL ligand (60.0 μM) or $Ni(BF_4)_2$ (60.0 μM) to replace the redox catalyst Ni-YL, no H_2 could be detected under the same reaction conditions.

An inhibition experiment was performed by adding a non-reactive species, namely, $[Fe(dcbpy)_3]$, into the reaction mixture.[23] The volume of the hydrogen produced in the presence of $[Fe(dcbpy)_3]$ (2.0 mM) was only 12.2% of that from the original system under the same experimental conditions (Figure 5c). Because the $[Fe(dcbpy)_3]$ did not quench the luminescence of the $[Ru(dcbpy)_3]$, the competitive inhibition behavior further confirmed that the PET process between $[Ru(dcbpy)_3]$ and Ni-YL occurred within the pocket of the Ni-YL cylinder by a typical enzymatic fashion in a more efficient way.[24] It should also be noted that the addition of $[Fe(dcbpy)_3]$ (0.1 mM) to a solution mixture containing $[Ru(dcbpy)_3]$ (10.0 μM) and Ni-YL (50 μM) resulted in an emission recovery of the same band. Such a recovery of the emission of $[Ru(dcbpy)_3]$ also indicative for the substitution of encapsulated $[Ru(dcbpy)_3]$ molecules in the pocket of the molecular cylinder Ni-YL by the inhibitor $[Fe(dcbpy)_3]$. When we irradiated the aforementioned $[Ru(dcbpy)_3]$ (2.0 mM)/Ni-ML (60.0 μM)/TEOA (15%) system, about 0.26 mL of hydrogen were produced after 5 h of irradiation. Besides, the addition of the corresponding concentration of $[Fe(dcbpy)_3]$ did not change much the volume of the produced hydrogen, and also could hardly recover the emission intensity. These results indicate the advantage of the supramolecular system on this light-driven reaction.

Conclusion

In summary, a hexanuclear metal–organic cylinder based on redox-active Ni^{II} centers was prepared through the coordination of metal–organic assemblies. Owing to the introduction of amide groups and secondary amine groups, together with the design of a fixable backbone, the complex Ni-YL possesses a large cavity and diversified acting sites with the capability of encapsulating size-suitable anionic $[Ru(dcbpy)_3]$ showing an obvious host–guest behavior in solution. Optical measurements and control experiments reveal a pseudo-intramolecular PET between the $[Ru(dcbpy)_3]$ and the Ni-YL host, which leads to an efficient light-driven hydrogen production based on this system. These results suggest that our supramolecular system favors a pseudo-intramolecular PET process, showing a bright future as artificial photosynthetic systems for efficient photocatalytic reactions.

Experimental Section

Materials and methods: All chemicals were of reagent grade quality obtained from commercial sources and used without further purification. The photosensitizer $[Ru(dcbpy)_3]$ and $[Fe(dcbpy)_3]$ with the same configuration were prepared following literature methods.[25,26] The elemental analyses of C, H and N were performed on a Vario EL III elemental analyzer. ^{1}H NMR spectra were measured on a Varian INOVA 500M spectrometer. ESI mass spectra were carried out on a HPLC-Q-Tof MS spectrometer by using methanol as the mobile phase. The solution fluorescent spectra were measured on a JASCO FP-6500 spectrometer. Both excitation and emission slit widths were 5 nm. The solution of Ni-YL was prepared in CH_3CN with a concentration of 1 mM. Stock solutions of $[Ru(dcbpy)_3]$ (1 mM) were prepared directly in methanol with some addition of NaOH to pH 10.5 for the test of fluorescence titration and transient absorption measurements. The electrochemical studies were measured on a CHI 1130 (CH Instrument Co., Shanghai) electrochemical analyzer under nitrogen at room temperature by using Ag/AgCl electrode as a reference electrode, a platinum silk with 0.5 mM diameter as a counter electrode, and a glassy carbon electrode as a working electrode. The nanosecond time-resolved transient difference absorption spectra were obtained by using an Edinburgh LP920 instrument (Edinburgh Instruments, UK).

For the photoinduced hydrogen evolution,[27] the system was irradiated by using a 500 W Xenon lamp; the reaction temperature was 298 K by using a water filter to absorb heat. The flask was sealed with a septum and degassed by bubbling argon for 30 min under atmospheric pressure at room temperature. The pH value of the system was adjusted to a specific pH by adding HCl or NaOH and was measured with a pH meter. The generated photoproduct of H_2 was characterized by using GC 7890T instrument analysis by using a 5 Å molecular sieve column (0.6 m × 3 mm), a thermal conductivity detector, and nitrogen was used as carrier gas. The amount of hydrogen generated was determined by the external standard method. Hydrogen in the resulting solution was not measured and the slight effect of the hydrogen gas generated in the pressure of the flask was neglected for calculation of the volume of hydrogen gas.

Preparation

(E)-Dimethyl 5-(4-(methoxycarbonyl)benzylideneamino)isophthalate (a): A mixture of dimethyl 5-aminoisophthalate (2.09 g, 10 mmol) and methyl 4-formylbenzoate (1.64 g, 10 mmol) was dissolved in methanol solution (100 mL), then the solution was heated to reflux overnight after five drops of acetic acid were added. The white product was collected by filtration and washed with methanol several times. Yield: 3.09 g, 82%. ^{1}H NMR ($CDCl_3$, 400 MHz): $\delta = 3.92$ (s, 3H; $COOCH_3$), 3.97 (d, $J = 3.4$ Hz, 6H; $COOCH_3$), 7.52 (d, $J = 1.2$ Hz, 1H; ArH), 7.92–8.07 (m, 3H; ArH), 8.09 (d, $J = 1.4$ Hz, 1H; ArH), 8.19 (dd, $J = 14.9$, 8.2 Hz, 2H; ArH), 8.58 ppm (s, 1H; CH).

Dimethyl 5-(4-(methoxycarbonyl)benzylamino)isophthalate (b): (*E*)-Dimethyl 5-(4-(methoxycarbonyl) benzylideneamino)isophthalate (1.77 g, 5 mmol) and $NaBH_4$ (0.23 g, 6 mmol) were added to dichloromethane (30 mL) and methanol (20 mL). After being stirred for 10 h at room temperature, diluted HCl (1.0 mol) was added to the solution to quench the reaction. The organic solvent was evaporated in vacuum and the pH value of the aqueous residue was adjusted to approximately 8–10 with a saturated aqueous solution of sodium bicarbonate, and then the aqueous phase was extracted with ethyl acetate to give crude desired compound as a solid. The residue was purified by silica gel column chromatography (ethyl acetate/dichloromethane 1:100). Yield: 1.42 g, 79%. ^{1}H NMR ($CDCl_3$, 400 MHz): $\delta = 3.90$ (s, 6H; $COOCH_3$), 3.91 (s, 3H; $COOCH_3$), 4.48 (s, 2H; CH_2), 7.43 (d, $J = 8.3$ Hz, 2H; ArH), 7.46 (d, $J = 1.4$ Hz, 2H; ArH), 7.98–8.06 ppm (m, 3H; ArH).

5-(4-(Hydrazinecarbonyl)benzylamino)isophthalohydrazide (c): A mixture solution of 80% hydrazine hydrate (5.25 g, 84 mmol) and dimethyl 5-(4-(methoxycarbonyl)benzylamino)isophthalate (0.5 g, 1.40 mmol) in methanol (30 mL) was stirred over 12 h at 70 °C. The precipitate was collected by filtration, washed with methanol, and dried in vacuum. Yield: 0.36 g, 72%. ^{1}H NMR ([D_6]DMSO, 400 MHz): $\delta = 4.39$ (d, $J = 6.0$ Hz, 2H; CH_2), 4.49 (d, $J = 39.9$ Hz, 6H; NH_2), 7.10 (s, 1H; ArH), 7.32–7.44 (m, 2H; ArH), 7.48 (d, $J = 7.8$ Hz, 1H; ArH), 7.76 (d, $J = 8.2$ Hz, 2H; ArH), 9.55 (s, 2H; CONH), 9.71 ppm (s, 1H; CONH).

Ligand YL: 5-(4-(Hydrazinecarbonyl)benzylamino)isophthalohydrazide (0.5 g, 1.40 mmol) was added to a solution of 2-pyridinecar-

boxaldehyde (0.495 g, 4.62 mmol) in methanol (40 mL). After five drops of acetic acid were added, the mixture was heated to reflux overnight at 70 °C. The yellow product was collected by filtration, washed with methanol, and dried in vacuum. Yield: 0.67 g, 70%. ^{1}H NMR ([D$_6$]DMSO, 400 MHz): δ = 3.83 (s, 1H; NH), 4.51 (d, J = 4.7 Hz, 2H; CH$_2$), 7.00 (s, 1H; CH=N),7.30 (d, J = 10.0 Hz, 2H; CH=N), 7.48–7.34 (m, 3H; ArH),7.54 (t, J = 9.4 Hz, 2H; ArH), 7.62 (s, 1H; ArH), 7.93 (s, 4H; ArH), 7.96 (t, J = 11.0 Hz, 3H; ArH), 8.44 (s, 1H; ArH), 8.47 (d, J = 11.3 Hz, 2H; ArH), 8.61 (d, J = 4.4 Hz, 3H; ArH), 12.01 (s, 1H; CONH), 12.08 ppm (s, 2H; CONH); elemental analysis calcd (%) for $C_{36}H_{28}N_{10}O_3$: H 4.35, C 66.65, N 21.59; found: H 4.40, C 66.89, N 21.32.

Ni-YL: A mixture of Ni(BF$_4$)$_2$·6H$_2$O (0.051 g, 0.150 mmol) and the ligand YL (0.093 g, 0.150 mmol) was dissolved in acetonitrile (20 mL) with strong stirring at 60 °C for 2 h. Then the solution was filtrated after being cooled to room temperature. Reddish block crystals were obtained through diffusing diethyl ether into the above-obtained filtrate after one week. Yield: 62% (based on the crystal dried in vacuum). Elemental analysis calcd (%) for $Ni_6(C_{204}H_{164}N_{60}O_{18})(BF_4)_8(CH_3CN)_3(H_2O)_7$: H 3.74, C 50.04, N 17.51; found: H 3.93, C 50.78, N 17.23.

Ni-ML: Phenylamine (0.028 g, 0.3 mmol), 2-pyridinecarboxaldehyde (0.032 g, 0.3 mmol), and Ni(BF$_4$)$_2$·6H$_2$O (0.034 g, 0.10 mmol) were dissolved in acetonitrile (20 mL). The reaction mixture was heated to reflux for one day at 70 °C. After cooling to room temperature, brown sliced crystals were obtained through diffusing diethyl ether into the above-obtained solution after two weeks. Yield: 65%. Elemental analysis calcd (%) for $Ni(C_{36}H_{30}N_6)(BF_4)_2(H_2O)_{0.5}$: H 3.96, C 54.87, N 10.66; found: H 3.88, C 55.02, N 9.74.

Crystallography: X-Ray intensity data were measured at 200(2) K on a Bruker SMART APEX CCD-based diffractometer ($Mo_{K\alpha}$ radiation, λ = 0.71073 Å) by using the SMART and SAINT programs.[28,29] The crystal data were solved by direct methods and further refined by full-matrix least-squares refinements on F^2 by using the SHELXL-97 software and an absorption correction was performed by using the SADABS program.[30] The non-hydrogen atoms were refined with anisotropic displacement parameters. The hydrogen atoms within the ligand backbones and the solvent CH_3CN molecules were fixed geometrically at calculated distances and allowed to ride on the parent non-hydrogen atoms. For Ni-YL, four fluorine atoms in two half occupied BF_4^- ions were disordered into two parts with each S.O.F. (site occupied factor) fixed as 0.25. The B–F bond length and the F–F distances of several BF_4^- ions were constrained to be the same, and the thermal parameters of adjacent atoms in these BF_4^- ions were constrained to be similar. For Ni-ML, three F atoms in the BF_4^- ions were disordered into two parts with each S.O.F. fixed as 0.5. The crystal data are listed in Table 1.

Table 1. Crystal data of Ni-YL and Ni-ML.[a]

Compound	Ni-YL	Ni-ML
empirical formula	$C_{210}H_{187}N_{63}O_{25}Ni_6B_8F_{32}$	$C_{36}H_{31}N_6O_{0.5}NiB_2F_8$
formula weight [g mol^{-1}]	5039.97	788.00
T [K]	200(2)	200(2)
crystal system	orthorhombic	triclinic
space group	$Fdd2$	$P\bar{1}$
a [Å]	62.337(8)	9.6501(12)
b [Å]	18.920(2)	19.591(2)
c [Å]	54.815(7)	20.506(3)
α [°]	90	113.857(9)
β [°]	90	95.885(9)
γ [°]	90	90.008(9)
V [Å^{-3}]	64651(14)	3523.1(7)
Z	8	4
D_{calcd} [Mg m^{-3}]	1.035	1.486
μ [mm^{-1}]	1.035	0.632
F(000)	20656	1612
R_{int}	0.1229	0.0980
data/parameters	28367/1781	12116/992
GOF	0.974	0.992
R [$I > 2\sigma(I)$][b]	R_1 = 0.0906, wR_2 = 0.1941	R_1 = 0.0874, wR_2 = 0.1727
R indices (all data)[c]	R_1 = 0.1901, wR_2 = 0.2244	R_1 = 0.1767, wR_2 = 0.1937
$\Delta\rho_{max,min}$ [e Å^{-3}]	0.573/−0.359	0.925/−0.881

[a] CCDC 1063216 (Ni-YL), 1063217 (Ni-ML) contain the supplementary crystallographic data for this paper. These data are provided free of charge by The Cambridge Crystallographic Data Centre. [b] $R_1 = \Sigma||F_o|-|F_c||/\Sigma|F_o|$. [c] $wR_2 = \Sigma[w(F_o^2-F_c^2)^2]/\Sigma[w(F_o^2)^2]^{1/2}$.

Acknowledgements

We gratefully acknowledge financial support from the NSFC (21531001, 21373036 and 21573034), and the Innovative Research Team in University (IRT1213).

Keywords: electron transfer · encapsulation · hydrogen · metal–organic cylinders · ruthenium

[1] R. F. Ludlow, S. Otto, *Chem. Soc. Rev.* **2008**, *37*, 101–108.
[2] S. Zarra, D. M. Wood, D. A. Roberts, J. R. Nitschke, *Chem. Soc. Rev.* **2015**, *44*, 419–432.
[3] a) W. M. Hart-Cooper, K. N. Clary, F. D. Toste, R. G. Bergman, K. N. Raymond, *J. Am. Chem. Soc.* **2012**, *134*, 17873–17876; b) Q. Zhang, K. Tiefenbacher, *J. Am. Chem. Soc.* **2013**, *135*, 16213–16219; c) Y. Jiao, J. Wang, P. Y. Wu, L. Zhao, C. He, J. Zhang, C. Y. Duan, *Chem. Eur. J.* **2014**, *20*, 2224–2231.
[4] Examples for organic macrocycles hosts: a) P. Mukhopadhyay, A. X. Wu, L. Isaacs, *J. Org. Chem.* **2004**, *69*, 6157–6164; b) W. Jiang, D. Ajami, J. Rebek Jr., *J. Am. Chem. Soc.* **2012**, *134*, 8070–8073; c) H. Y. Gan, B. C. Gibb, *Chem. Commun.* **2012**, *48*, 1656–1658; d) A. Ikeda, S. Shinkai, *Chem. Rev.* **1997**, *97*, 1713–1734; e) T. Brotin, J. P. Dutasta, *Chem. Rev.* **2009**, *109*, 88–130; f) M. N. Berberan-Santos, P. Choppinet, A. Fedorov, L. Jullien, B. Valeur, *J. Am. Chem. Soc.* **2000**, *122*, 11876–11886; g) E. A. Meyer, R. K. Castellano, F. Diederich, *Angew. Chem. Int. Ed.* **2003**, *42*, 1210–1250; *Angew. Chem.* **2003**, *115*, 1244–1287.
[5] a) M. Yoshizawa, M. Tamura, M. Fujita, *Science* **2006**, *312*, 251–254; b) P. Mal, B. Breiner, K. Rissanen, J. R. Nitschke, *Science* **2009**, *324*, 1697–1699; c) M. D. Pluth, R. G. Bergman, K. N. Raymond, *Science* **2007**, *316*, 85–88.
[6] a) A. Jiménez, R. A. Bibeisi, T. K. Ronson, S. Zarra, C. Woodhead, J. R. Nitschke, *Angew. Chem. Int. Ed.* **2014**, *53*, 4556–4560; *Angew. Chem.* **2014**, *126*, 4644–4648; b) K. Mahata, P. D. Frischmann, F. Würthner, *J. Am. Chem. Soc.* **2013**, *135*, 15656–15661; c) C. J. Hastings, M. P. Backlund, R. G. Bergman, K. N. Raymond, *Angew. Chem. Int. Ed.* **2011**, *50*, 10570–10573; *Angew. Chem.* **2011**, *123*, 10758–10761; d) D. M. Kaphan, F. D. Toste, R. G. Bergman, K. N. Raymond, *J. Am. Chem. Soc.* **2015**, *137*, 9202–9205; e) M. Otte, P. F. Kuijpers, O. Troeppner, I. Ivanović-Burmazović, J. N. H. Reek, B. de Bruin, *Chem. Eur. J.* **2014**, *20*, 4880–4884; f) A. H. Chughtai, N. Ahmad, H. A. Younus, A. Laypkov, F. Verpoort, *Chem. Soc. Rev.* **2015**, *44*, 6804–6849.
[7] a) M. L. Singleton, J. H. Reibenspies, M. Y. Darensbourg, *J. Am. Chem. Soc.* **2010**, *132*, 8870–8871; b) G. Ghale, V. Ramalingam, A. R. Urbach, W. M. Nau, *J. Am. Chem. Soc.* **2011**, *133*, 7528–7535; c) X. Jing, C. He, Y. Yang, C. Y. Duan, *J. Am. Chem. Soc.* **2015**, *137*, 3967–3974.
[8] P. D. Frischmann, K. Mahata, F. Würthner, *Chem. Soc. Rev.* **2013**, *42*, 1847–1870.

[9] C. K. Prier, D. A. Rankic, D. W. C. MacMillan, *Chem. Rev.* **2013**, *113*, 5322 – 5363.
[10] a) C. He, Z. H. Lin, Z. He, C. Y. Duan, C. H. Xu, Z. M. Wang, C. H. Yan, *Angew. Chem. Int. Ed.* **2008**, *47*, 877 – 881; *Angew. Chem.* **2008**, *120*, 891 – 895; b) H. M. Wu, C. He, Z. H. Lin, Y. Liu, C. Y. Duan, *Inorg. Chem.* **2009**, *48*, 408 – 410.
[11] a) A. M. Stadler, J. Harrowfield, *Inorg. Chim. Acta* **2009**, *362*, 4298 – 4314; b) L. Zhao, S. Y. Qu, C. He, R. Zhang, C. Y. Duan, *Chem. Commun.* **2011**, *47*, 9387 – 9389.
[12] K. I. Assaf, W. M. Nau, *Chem. Soc. Rev.* **2015**, *44*, 394 – 418.
[13] J. Lagona, P. Mukhopadhyay, S. Chakrabarti, L. Isaacs, *Angew. Chem. Int. Ed.* **2005**, *44*, 4844 – 4870; *Angew. Chem.* **2005**, *117*, 4922 – 4949.
[14] a) H. Tang, D. Fuentealba, Y. H. Ko, N. Selvapalam, K. Kim, C. Bohne, *J. Am. Chem. Soc.* **2011**, *133*, 20623 – 20633; b) S. Ghosh, P. Mukhopadhyay, L. Isaacs, *J. Syst. Chem.* **2010**, *1*, 6.
[15] a) A. K. Rappe, C. J. Casewit, K. S. Colwell, W. A. G. III, W. M. Skiff, *J. Am. Chem. Soc.* **1992**, *114*, 10024 – 10035; b) Gaussian 09, Revision B.01, M. J. Frisch, G. W. Trucks, H. B. Schlegel, G. E. Scuseria, M. A. Robb, J. R. Cheeseman, G. Scalmani, V. Barone, B. Mennucci, G. A. Petersson, H. Nakatsuji, M. Caricato, X. Li, H. P. Hratchian, A. F. Izmaylov, J. Bloino, G. Zheng, J. L. Sonnenberg, M. Hada, M. Ehara, K. Toyota, R. Fukuda, J. Hasegawa, M. Ishida, T. Nakajima, Y. Honda, O. Kitao, H. Nakai, T. Vreven, J. A. Montgomery, Jr., J. E. Peralta, F. Ogliaro, M. Bearpark, J. J. Heyd, E. Brothers, K. N. Kudin, V. N. Staroverov, T. Keith, R. Kobayashi, J. Normand, K. Raghavachari, A. Rendell, J. C. Burant, S. S. Iyengar, J. Tomasi, M. Cossi, N. Rega, J. M. Millam, M. Klene, J. E. Knox, J. B. Cross, V. Bakken, C. Adamo, J. Jaramillo, R. Gomperts, R. E. Stratmann, O. Yazyev, A. J. Austin, R. Cammi, C. Pomelli, J. W. Ochterski, R. L. Martin, K. Morokuma, V. G. Zakrzewski, G. A. Voth, P. Salvador, J. J. Dannenberg, S. Dapprich, A. D. Daniels, O. Farkas, J. B. Foresman, J. V. Ortiz, J. Cioslowski, and D. J. Fox, Gaussian, Inc., Wallingford CT, **2010**.
[16] A. D. Wilson, R. H. Newell, M. J. McNevin, J. T. Muckerman, M. R. DuBois, D. L. DuBois, *J. Am. Chem. Soc.* **2006**, *128*, 358 – 366.
[17] K. Swarnalatha, E. Rajkumar, S. Rajagopal, R. Ramaraj, Y. L. Lu, K. L. Lu, P. Ramamurthy, *J. Photochem. Photobiol. A* **2005**, *171*, 83 – 90.
[18] a) E. Rajkumar, S. Rajagopal, *Photochem. Photobiol. Sci.* **2008**, *7*, 1407 – 1414; b) J. I. Goldsmith, W. R. Hudson, M. S. Lowry, T. H. Anderson, S. Bernhard, *J. Am. Chem. Soc.* **2005**, *127*, 7502 – 7510.
[19] D. Thiruppathi, P. Karuppasamy, M. Ganesan, V. K. Sivasubramanian, T. Rajendran, S. Rajahopal, *J. Photochem. Photobiol. A* **2014**, *295*, 70 – 78.
[20] R. J. Holbrook, D. J. Weinberg, M. D. Peterson, E. A. Weiss, T. J. Meade, *J. Am. Chem. Soc.* **2015**, *137*, 3379 – 3385.
[21] H. F. M. Nelissen, M. Kercher, L. De Cola, M. C. Feiters, R. J. M. Nolte, *Chem. Eur. J.* **2002**, *8*, 5407 – 5414.
[22] M. P. McLaughlin, T. M. McCormick, R. Eisenberg, P. L. Holland, *Chem. Commun.* **2011**, *47*, 7989 – 7991.
[23] C. He, J. Wang, L. Zhao, T. Liu, J. Zhang, C. Y. Duan, *Chem. Commun.* **2013**, *49*, 627 – 629.
[24] C. J. Hastings, D. Fiedler, R. G. Bergman, K. N. Raymond, *J. Am. Chem. Soc.* **2008**, *130*, 10977 – 10983.
[25] S. Q. Zhang, L. Han, L. N. Li, J. Cheng, D. Q. Yuan, J. H. Luo, *Cryst. Growth Des.* **2013**, *13*, 5466 – 5472.
[26] C. M. Elliott, *Langmuir* **2005**, *21*, 3022 – 3027.
[27] P. Zhang, M. Wang, Y. Na, X. Li, Y. Jiang, L. Sun, *Dalton Trans.* **2010**, *39*, 1204 – 1206.
[28] SMART Data collection software, version 5.629; Bruker AXS Inc.: Madison, WI, **2003**.
[29] SAINT Data reduction software, version 6.45; Bruker AXS Inc.: Madison, WI, **2003**.
[30] SHELX-97: Program for crystal structure analysis, G. M. Sheldrick, University of Göttingen, Göttingen (Germany), **1997**.

Received: December 10, 2015
Published online on February 29, 2016